Biochimica et Biophysica Acta 1828 (2013) 365–372

Contents lists available at SciVerse ScienceDirect

Biochimica et Biophysica Acta

journal homepage: www.elsevier.com/locate/bbamem

Changes of cell electrical parameters induced by electroporation. A dielectrophoresis study

Mihaela G. Moisescu [a], Mihai Radu [a,b,*], Eugenia Kovacs [a], Lluis M. Mir [c,d,e], Tudor Savopol [a]

[a] Carol Davila Medical University, Biophysics and Cell Biotechnology Department, P.O. Box 35-43, Bucharest, Romania
[b] Horia Hulubei National Institute for Physics and Nuclear Engineering, Life and Environmental Physics Department, P.O. Box MG-6, Bucharest-Magurele, Romania
[c] Université Paris-Sud, UMR 8203, Laboratoire de Vectorologie et Thérapeutiques, Anticancéreuses, Orsay, F-91405, France
[d] CNRS, UMR 8203, Orsay, F-91405, France
[e] Institut Gustave Roussy, UMR 8203, Villejuif F-94805, France

ARTICLE INFO

Article history:
Received 28 March 2012
Received in revised form 27 August 2012
Accepted 31 August 2012
Available online 19 September 2012

Keywords:
Dielectrophoresis
Electropermeabilization
Cell dielectrical properties
Single shell model
Crossover frequency

ABSTRACT

Dielectrophoresis was employed to distinguish the electroporated from non-electroporated cells. It was found that the electric field frequency at which cells change the direction of their movement (the crossover frequency f_{CO}) is higher when cells are electroporated. The contribution to the cell dielectrophoretic behavior of four electric and geometrical cell parameters was analyzed using a single shell model. f_{CO} measurements were performed in media with conductivities of 0.001–0.09 S/m, on B16F10 cells which were electroporated in a Mannitol solution (0.001 S/m), using rectangular or exponential pulses. The control cells' f_{CO} was found in a domain of 2 to 105 kHz, while the electroporated cells' f_{CO} was in a domain of 5 to 350 kHz, depending on the external media conductivities. At exterior conductivities above ~0.02 S/m, f_{CO} of electroporated cells became significantly higher compared to controls. Even though the possible contribution of membrane permittivity to explain the observed f_{CO} shift toward higher values cannot be excluded, the computations highlight the fact that the variation of cytosol conductivity might be the major contributor to the dielectrophoretic behavior change. Our experimental observations can be described by considering a linear dependence of electroporated cells' cytosol conductivity against external conductivity.

1. Introduction

Nowadays cell electroporation is widely used to induce cellular transfection and to enhance the penetration of cytotoxic drugs into cancer cells (electrochemotherapy). A single or a series of electric pulses of appropriate amplitude and duration are able to reversibly permeabilize the cell membrane allowing impermeable molecules to access the intracellular compartments (e.g., DNA [1,2], drugs [3,4]). The molecular mechanisms of an electric-induced increase in cell membrane permeability are under debate, and the electrical state of the cell after poration being still an open question. There are reports showing that the electroporation pulses change the cell parameters (e.g., membrane conductivity) depending on the pulse amplitude and its duration [5\]. There are also reports regarding the lifetime of the permeabilized state of the membrane, suggesting that the membrane is highly permeable for some minutes depending on the temperature (<5 min at room temperature) [6]. For low external conductivities (<0.1 S/m), the amplitude of the permeabilization process is modulated by the ionic strength of the buffer in which the cells are electrically porated [7]. Changes in buffer conductivity have been observed during and immediately after electroporation [8] showing that a leakage of ions occurs from the cells during the highly permeabilized state of the membrane.

In this context, our work focused on the possibility of using dielectrophoretic crossover frequency recorded in media of various conductivities, as a tool for identifying changes in the electrical parameters of electroporated cells.

Based on the interfacial polarization induced by periodic electric fields, there are several efficient methods for mechanical manipulation of biological cells which have been described: dielectrophoresis (DEP) [9], electrorotation [10] and electroorientation [11]. Extensive practical and theoretical studies have been devoted to these techniques resulting in many medical and biotechnological applications, especially for DEP, e.g. cell therapeutics, drug discovery, biosensors, medical diagnostics, nanoassembly, and particle separation [12]. In particular, the ability of DEP to separate cells with different electrical characteristics (according to their direction and velocity of movement) has been largely exploited in the last few years through integrating DEP capabilities into microfluidic devices called "lab on chip" platforms [12].

* Corresponding author at: Carol Davila Medical University, Biophysics and Cell Biotechnology Department, P.O. Box 35-43, Bucharest, Romania. Tel./fax: +40 213125955.
E-mail address: mradu@nipne.ro (M. Radu).

0005-2736/$ – see front matter © 2012 Elsevier B.V. All rights reserved.
http://dx.doi.org/10.1016/j.bbamem.2012.08.030

Two types of DEP-controlled movements have been theoretically described and experimentally observed: positive (pos-DEP) and negative dielectrophoresis (neg-DEP) (as cell moves respectively, toward or against a high intensity region of the field), each of them occurring in a characteristic range of electric field frequencies. The switch between pos-DEP and neg-DEP occurs at a specific frequency called the *critical* or *crossover frequency* (f_{CO}) [13–16]. In a mixture of cells having different f_{CO}'s, the separation of cell categories becomes possible as a result of the proper selection of a field frequency which simultaneously induces pos- or neg-DEP to either category of cells. This procedure had already proved efficient in the case of bacteria separation [13]; when differentiating molecular effects on erythrocyte membrane [14]; when separating human lymphocyte fractions [17]; in selecting mammalian cells based on their cell-cycle phase [18]; for the selective trapping of live and dead cells [19], or when distinguishing stem cells and their differentiated progeny [20], etc.

In our work we show that f_{CO} recordings may be used to understand the mechanisms of cell electrical behavior changes induced by electroporation as well as for separating electroporated from control cells.

2. Computations of crossover frequency

The single shell model [21–23] was used to account for the dielectrophoretic behavior of electroporated cells. This model simplifies a nucleated cell to a spherical, homogeneous particle of an equivalent radius (r), where only the cytoplasmic membrane is represented by a shell of given thickness (d), and which employs effective values for the complex permittivity ($\hat{\varepsilon}_p$) or conductivity ($\hat{\sigma}_p$) (p index stands for particle).

In a nonuniform electric field the DEP force (F_{DEP}) [24] is given by:

$$F_{DEP=}2\pi^3\varepsilon_e \mathrm{Re}(CM)\nabla E^2 \quad (1)$$

where ε is the absolute permittivity, e index stands for external medium, E is the electrical field's intensity, and Re (CM) is the real part of the Clausius Mossotti factor (this describes the F_{DEP} dependence on the field frequency and on the geometrical and electric parameters of the particle, see Eqs. (2) and (3)). When nonuniform AC fields are applied to living cells, the conduction losses due to the mobile ions present in their structures and in the suspending medium, are accommodated into the single shell model by using the factor CM given by [12]:

$$CM(\omega) = \frac{\hat{\varepsilon}_p - \hat{\varepsilon}_e}{\hat{\varepsilon}_p + 2\hat{\varepsilon}_e} \qquad \left(\hat{\varepsilon} = \varepsilon_0\varepsilon - \frac{j\sigma}{\omega}\right) \quad (2)$$

where ω is the field's angular frequency ($\omega = 2\pi f$, f is the AC field frequency), ε_0 is the vacuum permittivity, j is the imaginary vector ($j = \sqrt{-1}$) and

$$\hat{\varepsilon}_p = \frac{\left(\frac{r}{r-d}\right)^3 + 2\left(\frac{\hat{\varepsilon}_i - \hat{\varepsilon}_m}{\hat{\varepsilon}_i + 2\hat{\varepsilon}_m}\right)}{\left(\frac{r}{r-d}\right)^3 - \left(\frac{\hat{\varepsilon}_i - \hat{\varepsilon}_m}{\hat{\varepsilon}_i + 2\hat{\varepsilon}_m}\right)} \quad (3)$$

(i and m indices stand for the particle interior and shell membrane, respectively).

The DEP spectrum (i.e., dependence of F_{DEP} on f) was actually given by the frequency dependence of Re(CM). Based on the above equations and using a MATLAB v7.7 script, the sign of Re(CM) was evaluated for a large frequency range (10^2–10^{10} Hz). The f_{CO} values were considered as the lowest frequency values at which the sign of Re(CM) changed. In order to understand how different cellular and extracellular parameters influence the experimentally observed f_{CO}, simulations of f_{CO} dependence on these parameters have been done. In Table 1 the parameters used in our simulations are shown.

3. Materials and methods

3.1. Cells

B16F10 murine melanoma cells were cultured at 37 °C, 5% CO_2 in Earle's Minimum Essential Medium w L-Glutamine (Gibco, Cergy-Pontoise, France) supplemented with 100 U/ml penicillin, 100 mg/ml streptomycin (Gibco), and 10% fetal bovine serum (Gibco). The cells were subcultured in 40×11 mm Petri dishes (TPP, Switzerland) for 24 h and reached subconfluence on the day of the experiment. The cells were harvested by trypsinization (Trypsin 0.25%/EDTA, Gibco). The extracellular conductivity was decreased by 3 consecutive centrifugations (200×g, 3 min) in 8 ml Mannitol solution.

3.2. Chemicals and media

All solutions were prepared in MilliQ ultrapure water (Millipore Co., EU) (18.2 MΩ×cm at 25 °C).

The 0.37 μM water stock of Propidium Iodide (PI) (Fluka BioChemika, USA) was stored at 4 °C in the dark and was diluted to 3.7 nM in all experiments.

The 300 mM D-Mannitol solution (Fluka), pH 7.2 ± 0.2, conductivity (σ_{M1}) 0.001 ± 0.0002 S/m and sucrose-based buffer (8 mM Na_2HPO_4, 2 mM KH_2PO_4, 1 mM $MgCl_2$, 250 mM sucrose) (25), pH 7.4 ± 0.01, conductivity (σ_{M11}) 0.125 ± 0.012 S/m were used as the basic media. Nine other media with different conductivities were prepared by mixing Mannitol solution with a sucrose-based buffer in different proportions: the media were numbered M_1 to M_{11} (including the basic ones) and had conductivities (σ_{Mi}) of 0.001, 0.005, 0.011, 0.022, 0.033, 0.044, 0.055, 0.075, 0.105, 0.115 and 0.125 S/m, respectively. The preparation variability reflected in the medium conductivity was under 15%. All buffers were isotonic (304 ± 4 mOsmol/kg as it was checked with an Osmomat 030-RS, Gonotec, Germany).

3.3. Electroporation experiments

Two types of electric pulses delivered as a succession of 8 pulses (1 Hz repetition frequency) were used to permeabilize the cells. There were rectangular pulses (1.2, 1.5 and 1.8 kV/cm, 100 μs pulse duration, using a Cliniporator, IGEA, Carpi, Italy) or exponentially-decaying pulses (2.5 kV/cm, 100 μs time constant, using a Multiporator, Eppendorf, Hamburg, Germany).

Cells in Mannitol (1–3×10^6 cells/ml) were permeabilized using cuvettes with 2 mm gap aluminum electrodes (Cell Projects Ltd., Harrietsham, UK). PI was added before the delivery of pulses or before sham exposures.

3.4. FACS analysis

Cells were prepared for electroporation and the analysis was done within 10 min after poration. A total of 10^4 cells per sample were checked for PI uptake using a FACScan flow cytometer (Becton-

Table 1
Geometric and electric parameters used in the single shell model describing the dielectrophoretic behavior of cells.

Parameter	Symbol	Value	Unit	Reference
Medium conductivity	σ_e	0.001–0.1	S/m	Measured
Medium permittivity[a]	ε_e	80	RU	[26]
Membrane conductivity	σ_m	10^{-7}	S/m	[21]
Membrane permittivity[a]	ε_m	12	RU	[39,40]
Membrane thickness	d	5×10^{-9}	m	[35]
Cytosol conductivity	σ_i	0.5	S/m	[35,33]
Cytosol permittivity[a]	ε_i	60	RU	[24]
Cell radius	r	6×10^{-6}	m	Measured

[a] Relative dielectric permittivity.

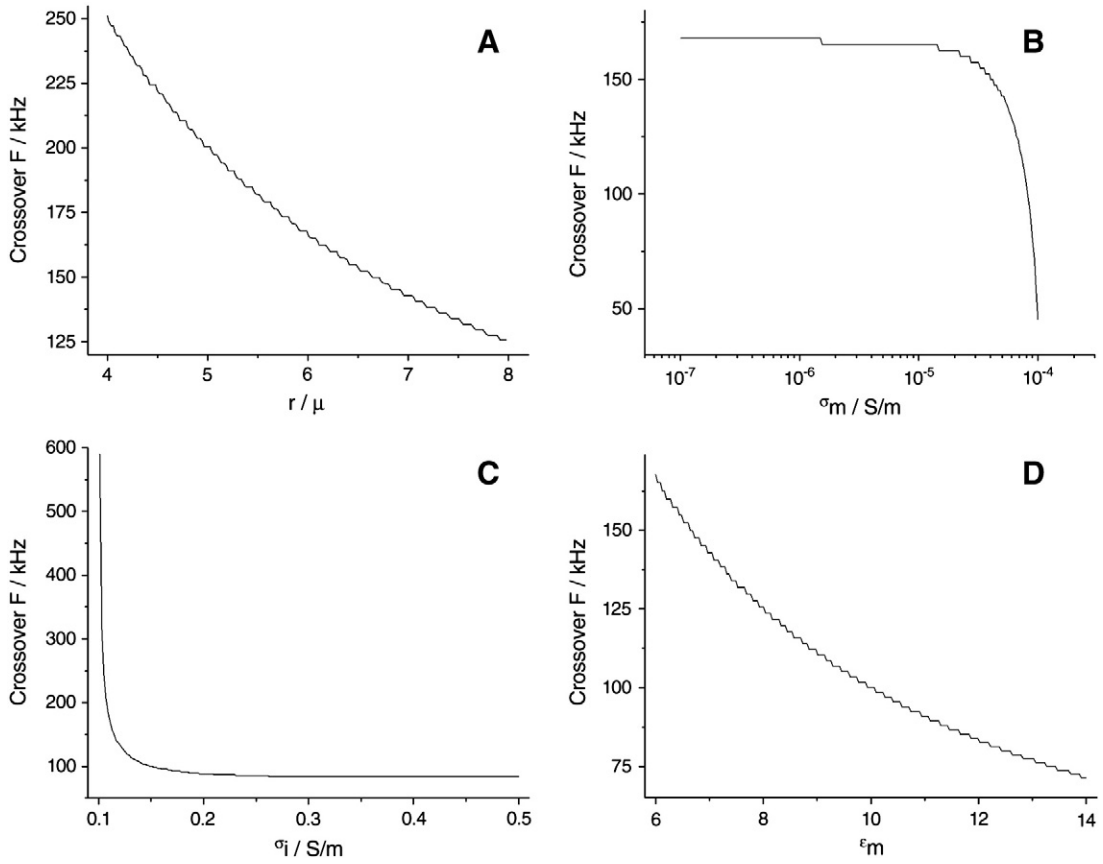

Fig. 1. Simulations of crossover frequency as a function of the following cellular parameters: A — cell radius, r; B — membrane conductivity, σ_m; C — cytosol conductivity, σ_i; D — membrane relative permittivity, ε_m. Standard values of electrical and geometrical parameters for nonporated cellular suspensions are listed in Table 1.

Dickinson, Franklin Lakes, NJ). For the evaluation of membrane resealing, PI was added 30 min after electroporation. In the meantime, the suspension was kept at room temperature and the cells were PI-incubated for 4 min before FACS measurements.

3.5. Cell diameter measurements

Cells were washed, electroporated and mixed with various media. Electroporation was performed in either low (M_1) or high (M_{11}) conductivity media, then cell suspensions were diluted 1:1 in M_1 or M_{11} medium, respectively. Within 2 min after pulse delivery, 10 μl of the final suspension was placed on a disposable counting chamber (Hirschmann Laborgerate GmbH, Eberstadt, Germany). Cell images (transmission and fluorescence, 40×) were acquired every minute for 15 min. Two perpendicular diameters of 5 to 11 cells were measured frame by frame and every experimental category was repeated 3 times.

3.6. Conductivity measurements

Cells were washed and suspended in Mannitol solution. After electroporation, an equal volume of Mannitol or higher conductivity medium (M_2–M_{11}) was added, and the conductivity of cell suspension ($1–3\times10^6$ cells/ml) was monitored for 10 min after each delivery of pulses (conductometer InoLab Cond, WTW, Weilheim, Germany).

3.7. Dielectrophoresis experiments

The DEP chamber consisted of two chrome parallel electrodes (1 μm thickness and 100 μm gap in between) laid down on glass by a sputtering technique.

Sinusoidal fields up to 170 V/cm (computed by dividing the applied voltage to the width between the electrodes) over the frequency range 1–500 kHz were applied (Generator 33250A, Agilent, USA) and monitored (Oscilloscope 9344, LeCroy, France).

Cells' DEP behavior was observed using an inverted microscope (AxioVert S100, Zeiss, Jena, Germany) equipped with a camera (AxioCam HRc, Zeiss). During DEP, images and movies were recorded under fluorescence and transmitted light using AXIOVISION Rel. 4.6.3.0 software (Zeiss).

After electroporation or sham exposure, PI-incubated cells were immediately diluted with an equal volume of Mannitol solution or of a higher conductivity medium (M_2 to M_{11}). 30 μl of the final suspension

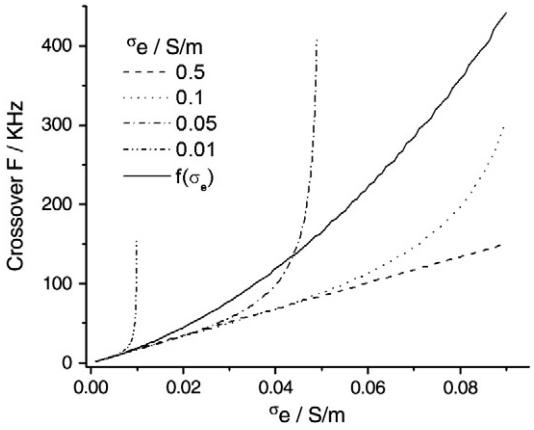

Fig. 2. Simulations of crossover frequency against external medium conductivity (σ_e) for cells with different cytosol conductivities (σ_i). The solid line stands for cells with a variable cytosol conductivity according to Eq. (4) (with $\alpha=0.012$, $\beta=0.98$, $\sigma_{i0}=0.5$ S/m).

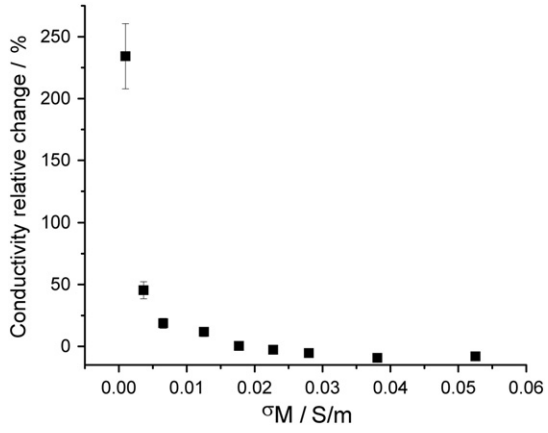

Fig. 3. Conductivity relative variations for electroporated cell suspensions when buffers of various conductivities (σ_{Mi}) were added after poration performed in low conductivity buffer (M_1) using 2.5 kV/cm exponentially-decaying pulses.

was loaded into a chamber and a DEP experiment was started 5 min after electroporation. Aliquots of cell suspension from the same batch of cells were loaded into the DEP chamber every ~5 min, but no later than 30 min after electroporation. Before each reloading, the electrodes were washed with MilliQ water and wiped down.

Cells' movement was registered as pos-DEP (toward electrodes) or neg-DEP (toward the center of the gap) when more than 90% of the cells present in the optical field moved in the specific direction. In case of mixed movements, both types of cell behavior were registered with positive or negative dominance. Dead and nonporated cells (as determined by fluorescence) were not considered.

After the cells' movements were recorded, the AC field was turned off and a new frequency was set. Cells were gently detached with a pipette tip from the electrodes and from each other and the AC field was turned on again for up to 10–15 s.

4. Results

4.1. Simulations of crossover frequency

The first f_{CO} was considered as the lowest frequency at which the sign of Re(*CM*) changed. The following parameters were considered in these simulations (Figs. 1 and 2):

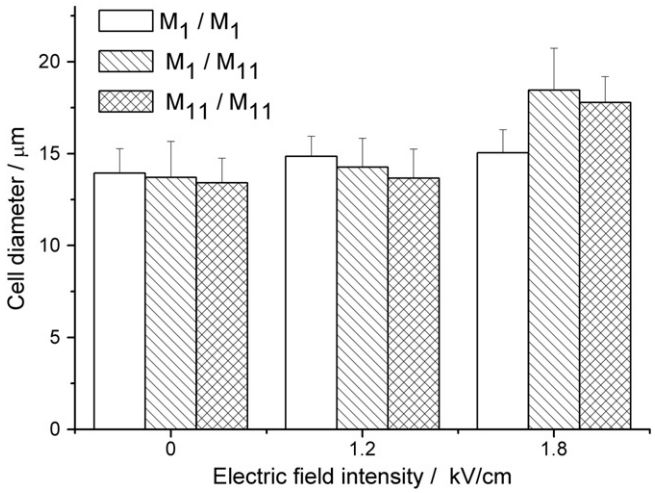

Fig. 4. B16F10 cells' diameters as a function of field intensity (1.2 and 1.8 kV/cm), measured 5 min after electroporation performed in low conductivity (M_1) buffer and diluted in either M_1 (*white* bars) or M_{11} (*diagonals* bars) buffers. Diameters of cells electroporated in a high conductivity buffer (M_{11}) and diluted in the same buffer are displayed in *diamond* bars.

i) *External medium conductivity* (σ_e) as an independent variable controlled during experiments;
ii) *Cell radius* (r) and *membrane* and *cytosol conductivities* and *membrane permittivity* (σ_m, σ_i, ε_m) which are susceptible to change after cell electroporation.

In our simulations *cytosol permittivity*, ε_i had no influence on the first f_{CO}, so no graph for this parameter was presented in Fig. 1.

The *external medium conductivity* strongly influenced the cell behavior in the domain of low and medium frequencies (first f_{CO} for normal cells increased from ~2 kHz to ~150 kHz for σ_e ranging between 0.001 and 0.09 S/m) (Fig. 2, dashed curve). This behavior enabled us to use the dependence of the first f_{CO} on σ_e to compare the electroporated cells with the controls.

Increasing the *cell radius* shifted the first f_{CO} toward lower values (Fig. 1A).

The influence of *membrane conductivity* on f_{CO} was almost insignificant even for σ_m of 2 orders of magnitude higher than those of an intact membrane; however, at $\sigma_m > 5\times10^{-5}$ S/m, f_{CO} started to shift toward lower values. At even higher values of σ_m the first f_{CO} drops very fast (Fig. 1B).

The *cytosol conductivity* influenced f_{CO} only if its value was very low (<0.15 S/m). When the values of σ_i become comparable to σ_e (close to 0.1 S/m), a rapid and sharp increase of the first f_{CO} can be observed (Fig. 1C).

The *membrane permittivity* had a direct influence on the first f_{CO}. The increase of ε_m in a reasonable range of values (from 6 to 14) shifted the f_{CO} toward lower values (Fig. 1D).

Another set of simulations was used for the calculation of f_{CO} for different *external medium* and *cytosol conductivities* (Fig. 2). For $\sigma_i = 0.5$ S/m (standard value for a cellular cytosol) f_{CO} increased almost linearly with σ_e on the investigated range (0.001 to 0.09 S/m). For 5, 10, and 50 times lower values of σ_i, there was a very sharp increase of f_{CO} with increasing σ_e. This sharp increase occurred when σ_e became comparable to σ_i.

The cells electroporated in low conductivity buffers are expected to present a decrease of σ_i due to the cell membrane's high permeability. Therefore, the behavior of f_{CO} as a function of σ_e was simulated based on the presumption of a linear dependence of σ_i on σ_e [25,26] using the function:

$$\sigma_i = \alpha\sigma_{i0} + \beta\sigma_e \tag{4}$$

where σ_{i0} is the control cytosol conductivity (0.5 S/m) and α and β are the coefficients that we determined in our experiments (see Fig. 6). The result is presented in Fig. 2 (solid line). f_{CO} nonlinearly increased with the exterior medium conductivity, but in a smoother manner.

4.2. External medium conductivity measurements

B16F10 cells were always electroporated in a low conductivity M_1 solution and diluted with either M_1 or higher conductivity buffers. Final conductivity was monitored up to 10 min after pulse delivery, although after 5 min no more increase of conductivity was observed (data not shown). Fig. 3 presents the relative change in cell suspension conductivity for porated cells (2.5 kV/cm) as a function of buffer conductivity (σ_{M1-M11}). Cell suspension conductivity increased very sharply when the cells were kept in a low conductivity solution (0.001 S/m). As expected, this increase vanished as the conductivity of the added buffer was higher.

4.3. Cell diameter

Diameter of B16F10 cells was measured after electroporation at 1.2 and 1.8 kV/cm performed either in low (M_1) or high (M_{11})

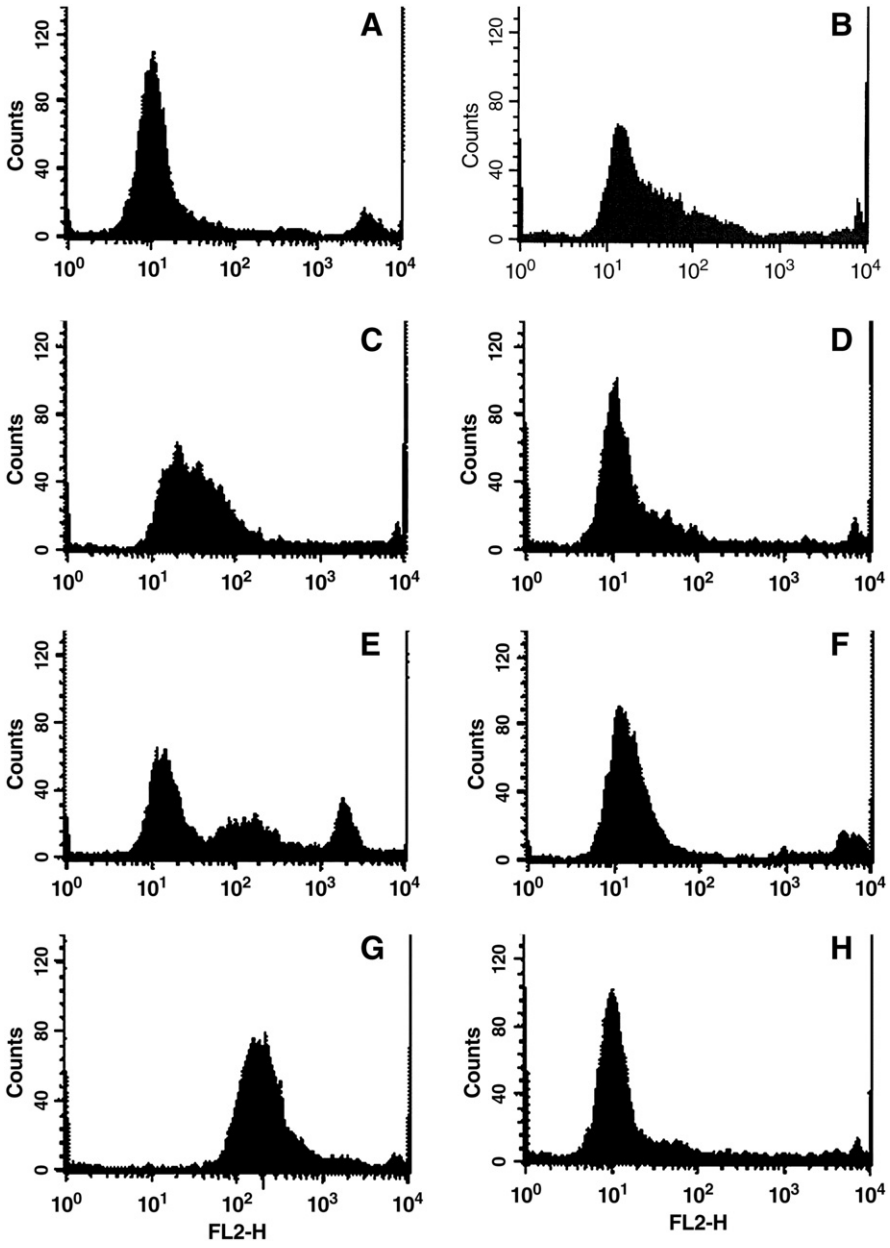

Fig. 5. Histograms of FACS analysis of B16F10 cells electroporated at different electric field intensities (rectangular pulses). Cells were electroporated in the presence of PI (*left* graphs, uptake process) and without PI (*right* graphs, resealing process, PI added 30 min after pulses delivery). Pulse amplitudes were: 0 kV/cm (A and B), 1.2 kV/cm (C and D), 1.5 kV/cm (E and F), and 1.8 kV/cm (G and H).

conductivity buffers (Fig. 4). The cell diameters for 3 different values of exterior buffer conductivities are presented: electroporation in M_1 and dilution with M_1 or with M_{11}, and electroporation in M_{11} and dilution with M_{11}.

The cell diameters were monitored under the microscope every minute for a period of up to 15 min. As long as the electroporation was performed in M_1, the cell diameters did not change significantly, even when the exterior medium conductivity was increased artificially by mixing the cell suspension with M_{11}. In the case of electroporation performed directly in M_{11}, the cells' diameters increased by about 30% in the high electric field.

4.4. FACS results

B16F10 cells' membrane permeabilization was confirmed in a flow-cytometer by PI uptake. Fig. 5 presents the histograms of fluorescence intensities of cells porated with pulses of 1.2, 1.5 and 1.8 kV/cm (Fig. 5C and D, Fig. 5E and F, and Fig. 5G and H, respectively). Cells were electroporated in the presence of PI (left panels) or in the absence of PI (right panels). For the latter, PI was added 30 min after the pulse delivery. Fluorescence histograms of controls for electroporation and resealing experiments are also presented (Fig. 5A and B).

With the increase of pulse amplitude, fluorescence intensities also gradually moved to higher values corresponding to the cell populations with the increased PI uptake (due to membrane permeabilization). Permeabilization proved to be reversible since no significant PI uptake was observed 30 min after pulse delivery in comparison with the controls.

4.5. Crossover frequency of control and electroporated cells

Fig. 6 presents f_{CO} as a function of σ_e for the control cells and for the cells electroporated with rectangular (Fig. 6A) and exponential pulses (Fig. 6B). In the case of the control cells, the f_{CO} showed a linear

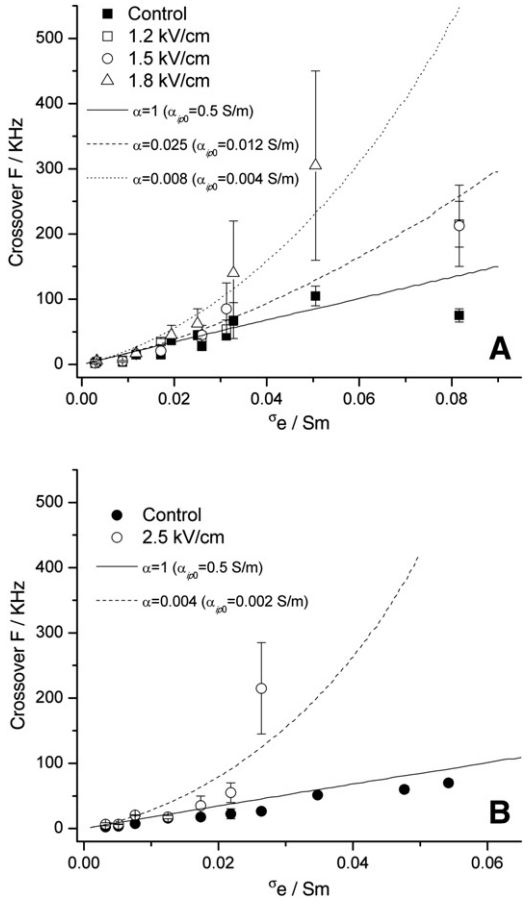

Fig. 6. Experimental (*symbols*) and simulated (*lines*) data for crossover frequency of B16F10 cells as a function of the exterior medium conductivity (σ_e) for control (*solid symbols*) and electroporated (*open symbols*) cells. A — Electroporation with rectangular pulses of amplitudes: 0 kV/cm (■), 1.2 kV/cm (□), 1.5 kV/cm (○), and 1.8 kV/cm (△); simulated curves: control (*solid line*) and electroporated cells with 1.2 and 1.5 kV/cm (*dash line*) and 1.8 kV/cm (*dot line*). B — Electroporation with exponential pulses of amplitudes: 0 kV/cm (●), and 2.5 kV/cm (○); simulated curves: control cells (*solid line*), cells electroporated with 2.5 kV/cm (*dash line*). The legend displays α coefficient of the linear function $\sigma_i = \alpha\sigma_{i0} + \beta\sigma_e$ ($\beta = 0.98$) used to simulate the cytosol conductivity of the electroporated cells (σ_i) against the external medium conductivity (σ_e) and the calculated cytosol conductivity (σ_{ip0}) after electroporation in a hypothetical *zero conductivity* buffer.

dependence on σ_e and ranged between 2.25 ± 0.75 and 105 ± 15 kHz. On the contrary, in the case of the electroporated cells, regardless of the pulse shape or amplitude, f_{CO} did not linearly increase with σ_e. A rapid evolution toward higher frequencies was observed. Cells displayed only neg-DEP in the following experimental conditions: $\sigma_e > 0.03$ S/m and 2.5 kV/cm exponential pulses; $\sigma_e > 0.05$ S/m and 1.8 kV/cm rectangular pulses; $\sigma_e > 0.09$ S/m and 1.2 or 1.5 kV/cm rectangular pulses.

Fig. 6 shows that the f_{CO} is higher for electroporated cells than for the controls, and follows an evolution similar to the predictions based on the hypothesis of a linear dependence of σ_i on σ_e (Fig. 2, solid curve). In the simulations superimposed on the experimental data, the cytosol conductivity was considered constant (0.5 S/m) for the control cells. For the electroporated cells, the simulations were done using the linear dependence of σ_i on σ_e presented in Eq. (4). The values of α coefficient are presented in Fig. 6. They strongly depend on the pulse amplitude. The α-values of 0.025 (for 1.2 and 1.5 kV/cm, rectangular pulses), 0.008 (for 1.8 kV/cm, rectangular pulses) and 0.004 (for 2.5 kV/cm, exponential pulses) better described the experimental data (Fig. 6). On the contrary, β coefficient seems to be independent on the electroporation conditions, having the same value (0.98) in all the curves describing the experimental data.

5. Discussion

According to our results, a clear shift of the f_{CO} toward higher frequencies occurs after cell electroporation.

The description of cellular dielectrophoresis in the frame of single shell model is based on the hypothesis that the polarization of cells is produced by the accumulation of electric charges at the interfaces (Maxwell Wagner polarization mechanism) [15,16,24]. According to this hypothesis, the time constant of the interfacial charge accumulation on the cell surface is supposed to be smaller in extracellular media with higher conductivities; consequently, the switch from neg-DEP to pos-DEP occurs at higher field frequencies. Consequently, an increase of the extracellular conductivity leads to a shift of the first f_{CO} toward higher values in agreement with the literature [18]. For this reason the dependence of f_{CO} on buffer conductivity was often used to characterize the DEP response of the cells [13,15]. Our experiments and simulations support this polarization mechanism (Figs. 2 and 6). The concept of f_{CO} was introduced for the first time by Jones [27] who gave also a general relation derived from the simple condition of $\mathrm{Re}(CM) = 0$. Because this equation is difficult to solve analytically, simplified versions of f_{CO} calculations were proposed in the literature, based on some restrictive conditions usually fulfilled when working with living cells [28,29]. On the other hand, in our experiments the cells exhibited a large change of electrical parameters of membrane and cytosol during and after electroporation. For this reason we preferred to numerically compute f_{CO} directly looking for the frequency value at which $\mathrm{Re}(CM) = 0$, (where $\mathrm{Re}(CM)$ changed the sign). In this way we avoided any approximation required by analytical formulas.

Considering the parameters investigated in our simulations one is geometrical (cell radius) and the other three are of electrical nature.

Increasing the cell radius (cell swelling) led to a slight shift of f_{CO} to lower values (Fig. 1A). Early papers on electroporation had reported cell swelling after pulse delivery [30–32]. The effect is usually explained by the fact that during the membrane permeabilization, an osmotic pressure results even in isotonic extracellular medium, due to the specific permeability of different ions and cytosolic macromolecules. This pressure drives water into the cell and leads to cellular colloid-osmotic swelling [31]. In all these reports, electroporation was performed in media with conductivities of 2–3 orders of magnitude higher than in our experiments. We found that cell diameters after electroporation were equivalent to those of the control cells if the pulse delivery was carried out in the lowest conductivity medium at 0.001 S/m (M_1). The cells' diameters increased significantly only if the electroporation was done in a medium (M_{11}) with a conductivity similar to the smallest value found in the literature (~0.1 S/m). The increase was ~30% which is almost the same as that reported by Golzio et al. on CHO cells [30]. Moreover, the cell diameter did not change even if the high conductivity medium (M_{11}) was added to the cells' suspensions electroporated in M_1.

Our DEP experiments have been performed 5 min after pulse delivery, and the cell diameter was not observed to change, regardless of the modifications of σ_e; nevertheless, an increase of f_{CO} occurred. Consequently, the observed f_{CO} shifts were not related to the cell size modifications.

Looking to the influence of membrane conductivity (Fig. 1B), the first f_{CO} is almost unchanged except, maybe, at very high σ_m, which is incompatible with living cells. Thus, the transient σ_m increase (induced by electroporation) cannot explain, by itself, the experimentally observed increase of f_{CO} (Fig. 6). The membrane resealing (which occurs, at room temperature, within 5 min [4,6]) should be also considered.

On the other hand, a decrease of ε_m of the electroporated cells in the investigated range ($6–14 \times \varepsilon_0$) shifts f_{CO} toward higher values. In fact, this explanation was already proposed in the case of similar experimental observations [33]. However, the value of ε_m needed to

produce these results had to be smaller than ε_0. Moreover, as molecular dynamics simulations show the penetration of water in the membrane during electroporation [34], the hydrophilic pores should lead to an enhancement of ε_m. However, since water seems to escape from the membrane according to a kinetic similar to that of its penetration (i.e., occurring within a few tens of nanoseconds), we used in our simulations the same value of ε_m for both electroporated and control cells.

Cytosol permittivity does not affect the first f_{CO} for values in a reasonable range (20–100$\times\varepsilon_0$) (data not shown).

Instead, σ_i in the range 0.1–0.5 S/m may influence the first f_{CO}. In the literature the usual value given for σ_i is 0.5 S/m [33,35]. Values going down close to external conductivity value (0.1 S/m in our simulation) produce a sharp increase of f_{CO} (Fig. 1C). This behavior was already mentioned in the literature [15,36] and is applicable to our experimental results.

In the electroporated cells, σ_i decreases due to the leakage of ions out of the cell during the pores' lifetime [8,32]. Considering the predicted dependence of f_{CO} on σ_i (Fig. 1C) we assume that the changes in ionic content of electroporated cells could thus be the main factor explaining our experimental results.

For the investigated range of σ_e the experimental recordings of f_{CO} for the control and the electroporated cells, showed a gradual increase. This pattern qualitatively reproduces the experimental results reported in the literature for other cell types [13,15]. The control cells had low f_{CO} which increased linearly with σ_e. The electroporated cells showed a nonlinear behavior of f_{CO} against σ_e. The values of f_{CO} were higher for the electroporated cells than for the controls at the same buffer conductivity, and the difference became significant for σ_e higher than ~0.02 S/m.

Our experimental data are well described by simulations where a linear dependence of σ_i of the electroporated cells on σ_e is assumed (Eq. (4)). As already mentioned, there is an ionic outflow due to electroporation which includes mainly potassium ions and leads to an increase of buffer conductivity [8,37]. In Pavlin's work, measurements of current through the cellular suspension during and after the pulses in a 0.127 S/m buffer, show an important increase of σ_e after 8 pulses [8]. After the membrane permeability recovery, a new σ_i value was reached, which depended on the initial conductivity gradient across the membrane, and on the permeabilization lifetime. Since the electroporation in our experiments has always been done in Mannitol buffer ($\sigma_e = 0.001$ S/m), the leakage of cytosol ion content was at its maximum during, and immediately after, the pulse delivery (Fig. 3). When adding buffers with increasing conductivities to the electroporated cells, σ_i reached increasing values which can be described by the α and β coefficients of Eq. (4). The slope (β coefficient) is not dependent on the intensity of the electric field, being very close to 1 regardless of the pulse amplitude. The y axis-intercept has the significance of σ_i which is reached in the extreme hypothetical case of poration in a *zero conductivity* buffer. In this case α represents the fraction of σ_i remaining in cells electroporated in this hypothetical *zero conductivity* buffer. As expected, this fraction diminishes if the pulse amplitude increases, suggesting a higher ion leakage. Cytosol conductivities after electroporation in this *zero conductivity* buffer might be thus calculated (see σ_{ip0}, Fig. 6) for an initial σ_i of 0.5 S/m. As expected, smaller σ_i were obtained, as higher pulse amplitudes caused larger defects in the cell membrane.

6. Conclusions

The f_{CO} measurements performed in the controlled extracellular media proved that DEP is a versatile tool to characterize the state of cells subjected to electroporation. Under our working conditions, f_{CO} for the control cells did not exceed 105 kHz while the f_{CO} of the electroporated cells ranged up to 350 kHz. f_{CO} of the electroporated cells was significantly higher than that of the controls for external conductivities above ~0.02 S/m. Cells electroporated with either rectangular or exponentially-decaying pulses can be thus separated from the non-electroporated ones based on their f_{CO} differences at appropriate external medium conductivities.

The theoretical predictions, based on the single shell model, highlighted the cytosol conductivity σ_i as the major contributor to the cell DEP behavior change after electroporation. During the electroporation in low conductivity buffers, an outflow of ions diminished σ_i leading to an f_{CO} increase for cells in the low and medium range of field frequencies (1–500 kHz). Our observations can be consistently explained by theoretical simulations, where a linear dependence of σ_i against the conductivity of the external buffer is assumed. However, we cannot totally exclude the possible contribution of membrane permittivity to explain the observed shift of f_{CO}.

Our experimental and theoretical results show that DEP is a promising investigation tool allowing insights into the electroporation mechanisms, as well as a practical application in separating electroporated cells based on their f_{CO} in microfluidic devices [17,38].

Acknowledgements

This paper is partially supported by: Sectoral Operational Programme Human Resources Development, financed by the European Social Fund and by the Romanian Government under the contract number POSDRU/89/1.5/S/64109, by CNCSIS-UEFISCSU, project number 1193 PNII-Idei code 1195/2008. The work was also performed in the frame of LEA EBAM. M.G. Moisescu and T. Savopol benefitted travel grants from PHC-Brancusi programme 494 and 495/2011.

We thank A. Sobetkii from MGM STAR CONSTRUCT SRL (Bucharest, Romania) for producing the dielectrophoresis chambers.

We thank the collaborators from Gustave Roussy Institute (Villejuif, France): J. Villemejane, F. André and E. Raeisi, and the collaborators from Carol Davila University (Bucharest, Romania): A.D. Barbut and L.O. Saplacan, for their technical support.

We thank Mina Graber for English revision.

References

[1] L.M. Mir, Nucleic acids electrotransfer-based gene therapy (electrogenetherapy): past, current, and future, Mol. Biotechnol. 43 (2009) 167.
[2] E. Neumann, M. Schaefer-Ridder, Y. Wang, P.H. Hofschneider, Gene transfer into mouse lyoma cells by electroporation in high electric fields, EMBO J. 1 (1982) 841.
[3] L.M. Mir, Bases and rationale of the electrochemotherapy, Eur. J. Cancer (Suppl. 4) (2012) 38.
[4] S. Orlowski, J. Belehradek Jr., C. Paoletti, L.M. Mir, Transient electropermeabilization of cells in culture. Increase of the cytotoxicity of anticancer drugs, Biochem. Pharmacol. 37 (1988) 4727.
[5] D. Walz, J. Teissie, G. Milazzo, Bioelectrochemistry of membranes, Bioelectrochemistry: Principles and Practice Series, vol. 6, Birkhäuser Verlag, Basel, Switzerland, 2012.
[6] M.P. Rols, J. Teissie, Electropermeabilization of mammalian cells to macromolecules: control by pulse duration, Biophys. J. 75 (1998) 1415.
[7] A. Ivorra, J. Villemejane, L.M. Mir, Electrical modeling of the influence of medium conductivity on electroporation, Phys. Chem. Chem. Phys. 12 (2010) 10055.
[8] M. Pavlin, M. Kanduser, M. Rebersek, G. Pucihar, F.X. Hart, R. Magjarevic, D. Miklavcic, Effect of cell electroporation on the conductivity of a cell suspension, Biophys. J. 88 (2005) 4378.
[9] H. Pohl, Dielectrophoresis, Cambridge University Press, Cambridge, 1978.
[10] R. Glaser, G. Fuhr, J. Gimsa, Rotation of erythrocytes, plant cells and protoplasts in an outside rotating electric field, St. Biophys. 96 (1983) 11.
[11] G. Schwarz, General equation for the mean electrical energy of a dielectric body in an alternating electrical field, J. Chem. Phys. 39 (1963) 2388.
[12] R. Pethig, Dielectrophoresis: status of the theory, technology, and applications, Biomicrofluidics 4 (2010) 022811.
[13] M. Castellarnau, A. Errachid, C. Madrid, A. Juarez, J. Samitier, Dielectrophoresis as a tool to characterize and differentiate isogenic mutants of *Escherichia coli*, Biophys. J. 91 (2006) 3937.
[14] J. Gimsa, T. Schnelle, G. Zechel, R. Glaser, Dielectric spectroscopy of human erythrocytes: investigations under the influence of nystatin, Biophys. J. 66 (1994) 1244.
[15] P. Marszalek, J.J. Zielinsky, M. Fikus, T.Y. Tsong, Determination of electric parameters of cell membranes by a dielectrophoresis method, Biophys. J. 59 (1991) 982.
[16] M. Radu, Effects of Variable Electric Fields on the Biological Cell Suspension, Babes-Bolyai University, Cluj-Napoca, Romania, 1999.
[17] J. Yang, Y. Huang, X.B. Wang, F.F. Becker, P.R. Gascoyne, Differential analysis of human leukocytes by dielectrophoretic field-flow-fractionation, Biophys. J. 78 (2000) 2680.

[18] U. Kim, C.W. Shu, K.Y. Dane, P.S. Daugherty, J.Y. Wang, H.T. Soh, Selection of mammalian cells based on their cell-cycle phase using dielectrophoresis, Proc. Natl. Acad. Sci. U. S. A. 104 (2007) 20708.
[19] C.P. Jen, T.W. Chen, Selective trapping of live and dead mammalian cells using insulator-based dielectrophoresis within open-top microstructures, Biomed. Microdevices 11 (2009) 597.
[20] L.A. Flanagan, J. Lu, L. Wang, S.A. Marchenko, N.L. Jeon, A.P. Lee, E.S. Monuki, Unique dielectric properties distinguish stem cells and their differentiated progeny, Stem Cells 26 (2008) 656.
[21] Y. Huang, R. Holzel, R. Pethig, X.B. Wang, Differences in the AC electrodynamics of viable and non-viable yeast cells determined through combined dielectrophoresis and electrorotation studies, Phys. Med. Biol. 37 (1992) 1499.
[22] M. Radu, Cellular electrorotation — a general theoretical model, St. Biophys. 137 (2012) 117.
[23] I. Turcu, C.M. Lucaciu, Dielectrophoresis: a spherical shell model, J. Phys. A: Math. Gen. 22 (1989) 985.
[24] Q. Hu, R.P. Joshi, A. Beskok, Model study of electroporation effects on the dielectrophoretic response of spheroidal cells, J. Appl. Phys. 106 (2009) 024701.
[25] M. Kriegmaier, M. Zimmermann, K. Wolf, U. Zimmermann, V.L. Sukhorukov, Dielectric spectroscopy of *Schizosaccharomyces pombe* using electrorotation and electroorientation, Biochim. Biophys. Acta 1568 (2001) 135.
[26] G. Pucihar, T. Kotnik, M. Kanduser, D. Miklavcic, The influence of medium conductivity on electropermeabilization and survival of cells in vitro, Bioelectrochemistry 54 (2001) 107.
[27] K.V. Kaler, T.B. Jones, Dielectrophoretic spectra of single cells determined by feedback-controlled levitation, Biophys. J. 57 (1990) 173.
[28] T.B. Jones, G.A. Kallio, Dielectrophoretic levitation of spheres and shells, J. Electrostat. 6 (1979) 207.
[29] Y. Huang, X.B. Wang, F.F. Becker, P.R. Gascoyne, Membrane changes associated with the temperature-sensitive P85gag-mos-dependent transformation of rat kidney cells as determined by dielectrophoresis and electrorotation, Biochim. Biophys. Acta 1282 (1996) 76.
[30] M. Golzio, M.P. Mora, C. Raynaud, C. Delteil, J. Teissie, M.P. Rols, Control by osmotic pressure of voltage-induced permeabilization and gene transfer in mammalian cells, Biophys. J. 74 (1998) 3015.
[31] K. Kinosita Jr., T.Y. Tsong, Formation and resealing of pores of controlled sizes in human erythrocyte membrane, Nature 268 (1977) 438.
[32] V.L. Sukhorukov, H. Mussauer, U. Zimmermann, The effect of electrical deformation forces on the electropermeabilization of erythrocyte membranes in low- and high-conductivity media, J. Membr. Biol. 163 (1998) 235.
[33] J. Oblak, D. Krizaj, S. Amon, A. ek-Lebar, D. Miklavcic, Feasibility study for cell electroporation detection and separation by means of dielectrophoresis, Bioelectrochemistry. 71 (2007) 164.
[34] Z.A. Levine, P.T. Vernier, Life cycle of an electropore: field-dependent and field-independent steps in pore creation and annihilation, J. Membr. Biol. 236 (2010) 27.
[35] W. Krassowska, P.D. Filev, Modeling electroporation in a single cell, Biophys. J. 92 (2007) 404.
[36] J. Gimsa, P. Marszalek, U. Loewe, T.Y. Tsong, Dielectrophoresis and electrorotation of neurospora slime and murine myeloma cells, Biophys. J. 60 (1991) 749.
[37] M. Pavlin, D. Miklavcic, Theoretical and experimental analysis of conductivity, ion diffusion and molecular transport during cell electroporation–relation between short-lived and long-lived pores, Bioelectrochemistry 74 (2008) 38.
[38] C. Iliescu, L. Yu, F.E.H. Tay, B. Chen, Bidirectional field-flow particle separation method in a dielectrophoretic chip with 3D electrodes, Sens. Actuators B: Chem. 129 (2008) 4971.
[39] S. Archer, H. Morgan, F.J. Rixon, Electrorotation studies of baby hamster kidney fibroblasts infected with herpes simplex virus type 1, Biophys. J. 76 (1999) 2833.
[40] X. Wang, F.F. Becker, P.R. Gascoyne, Membrane dielectric changes indicate induced apoptosis in HL-60 cells more sensitively than surface phosphatidylserine expression or DNA fragmentation, Biochim. Biophys. Acta 1564 (2002) 412.